Journal of Power Sources 196 (2011) 5746–5750

Contents lists available at ScienceDirect

Journal of Power Sources

journal homepage: www.elsevier.com/locate/jpowsour

Short communication

Synthesis and characterization of the iron/copper composite as an electrode material for the rechargeable alkaline battery

Chen-Yu Kao*, Yun-Ru Tsai, Kan-Sen Chou

Department of Chemical Engineering, National Tsing Hua University, Hsinchu 30013, Taiwan, R.O.C.

ARTICLE INFO

Article history:
Received 9 October 2010
Received in revised form
12 December 2010
Accepted 21 December 2010
Available online 7 January 2011

Keywords:
Iron electrode
Rechargeable alkaline battery
Nanoparticle
Composite

ABSTRACT

Iron/copper composite particles were synthesized by a chemical reduction method and then used as the anode material for a rechargeable alkaline battery. The particle size and structure of the samples were characterized by SEM and XRD. Their electrochemical performance was also studied. The results showed that the iron/copper composite prepared by this method is nanosized. Copper improves the electron transfer between particles, and the nanosized iron/copper composite not only has a high electrochemical capacity of up to 800 mAh g^{-1}(Fe to Fe(III)), but also has an excellent rate-capacity performance at a current density of 3200 mA g^{-1}. Compared with the iron nanoparticle without copper, the iron/copper composite sample maintains a smaller particle size during electrochemical cycling, and therefore improves the cycling stability of the iron electrode.

1. Introduction

Due to the limitation of natural resources, the development of alternative energy or the reduction of energy consumption are very important issues today. Developing an electrical vehicle or a hybrid electrical vehicle is a solution to save fossil fuel. The key factor here is to develop a large energy storage system to meet the demands of these devices. Besides the lithium ion battery, we believe that the Ni–Fe battery is one of the choices [1,2]. Ni–Fe batteries had ever been used for this purpose in 1910s because of its safety, long life cycle, low cost, environmental friendliness and good resistance against overcharge and deep discharge. However, the drawbacks of low energy density, low power density and high self-discharge rate are limited in their applications [3–5]. One of the reasons for the limited iron electrode capacity was due to the large size of iron particles prepared by the traditional methods [6]. During discharge, the passive film forms on the iron particle surface, which forbids the diffusion of the OH^- ion and also the transfer of the electron, and therefore stops the discharge reaction. When attempting to increase the capacity of iron electrodes, improving the utilization of iron particles is of priority concern. Iron electrodes, made by sintering, typically have a larger capacity than those made by pressing iron particles, because they have a better connection between the particles [7]. However, the capacity of the iron electrode remained at about 100–300 mAh g^{-1}; only one-third of the theoretical capacity of iron (962 mAh g^{-1}, first plaute). In our previous work, pure nanosized Fe particles were prepared successfully, and the nanosizing effect on the utilization of iron was investigated. The discharge capacity of iron nanoparticles could reach 700 mAh g^{-1} [8,9], but it dropped quickly to 170 mAh g^{-1} at the third cycle, suggesting poor reversibility of these nanoparticles all discharged to the insulator, $Fe(OH)_2$. Although many other investigators also tried nanosized iron active materials, the reversibility was not good. Therefore, more research was required to improve its cycling performance [10]. In our recent work, a conductive carbon black was added to the iron electrode to form a structure with a core of carbon-black and a shell of iron. The formation of a good conductive network of carbon black could improve the reversibility of the active material [11]. In this study, a different approach, by adding copper to iron, will be attempted to improve the electrical conductivity and hence the capacity of the Fe electrode in a Ni–Fe battery system [12].

2. Experimental

2.1. Synthesis of nanosized iron/copper material

A chemical reduction method was used to synthesize nanosized iron particles. Ferrous sulfate hydrate ($FeSO_4 \cdot 7H_2O$, Showa, Japan) of 0.025 mol was first dissolved in 200 ml D.I. water, followed by a dissolution of 0.05 mol of $NaBH_4$ (Lancaster, England) in 50 ml D.I. water. The $FeSO_4$ solution was then pumped into the ice-bathed $NaBH_4$ solution at a rate of 3 cm^3 min^{-1}. Here iron nanoparticles would be obtained, and they were then washed by hot water (>90 °C) and separated by a magnet three times.

* Corresponding author. Tel.: +886 3 5715131 33657; fax: +886 3 5725924.
E-mail address: d947625@oz.nthu.edu.tw (C.-Y. Kao).

0378-7753/$ – see front matter © 2011 Elsevier B.V. All rights reserved.
doi:10.1016/j.jpowsour.2010.12.076

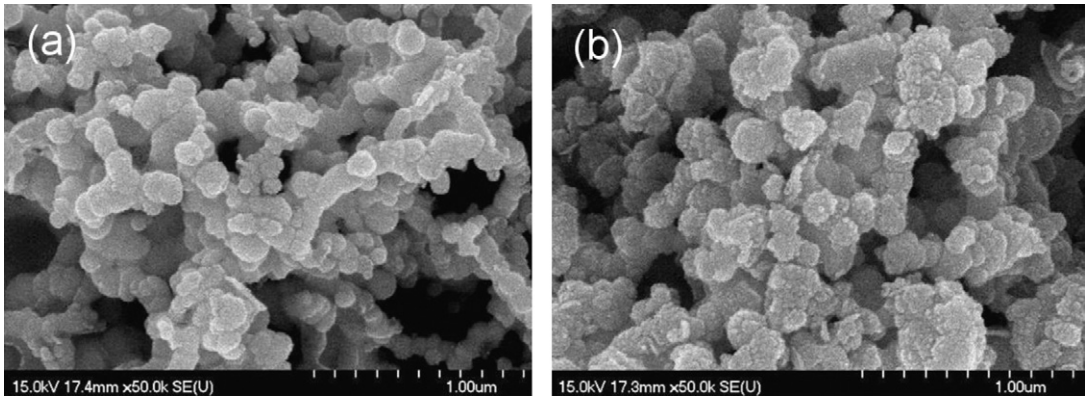

Fig. 1. The SEM images of the nanoparticles as prepared: (a) pure iron; (b) iron/copper composite (Fe:Cu = 3:1).

A typical method to synthesize the iron/copper composites is showed as follow. The obtained nanosized iron particles (0.025 mol of Fe) were dispersed again in 300 ml D.I. water under an ice bath. Copper sulfate hydrate ($CuSO_4 \cdot 5H_2O$, Showa, Japan) thoroughly in a weight ratio Fe:Cu = 1–10:1 were dissolved in 200 ml D.I. water, and then pumped into the nanosized iron particle solution at a rate of 3 cm^3 min^{-1}. After that, the $NaBH_4$ solution was then pumped into the above solution at 3 cm^3 min^{-1} to reduce all residual iron ions into nanoparticles; therefore, the composition of the composite is determined the same as iron and copper precursors. Finally, the as-prepared samples were washed by hot water (>90 °C) and separated by a magnet several times to obtain iron/copper composites.

2.2. Fabrication and electrochemical measurement of the iron/copper electrode

Performance of the active iron/copper material was measured by fabricating a paste type of nickel–iron cell system. The synthesized iron/copper active material, which contained 1.39 g of iron and a certain amount of copper, were mixed with 0.028 g of Na_2S (Showa, Japan) and 0.14 g of PTFE (60% suspended solution, Aldrich, USA) to form the pastes. Following the well-mixed process, fresh iron/PTFE mixtures were rapidly stuffed manually into the nickel foam (110 PPI, pores per inch, ShenYang Golden Champower New Material, China) to make an iron electrode. The nickel foam, 84 mm × 42 mm × 1.8 mm in size, was used not only to hold the iron/copper nanoparticles but also to collect the discharged current. Next, the iron electrodes were wrapped by non-woven PP cloth as separators. A miniature cell was assembled with a single iron electrode and two nickel electrodes with an excess capacity placed on both sides so that the cell performance would be limited by the iron electrode; the cell was then packed in a case. The electrolyte comprises of 8 M KOH and 1 M LiOH. A battery testing system (760B, Acutech System, Taiwan) was then used to evaluate the performance of the iron electrodes at room temperature. The cells would be cycled in the range of 0.8–1.65 V at a current density of 200 mA g^{-1}(Fe).

2.3. Characterization

After a certain discharge/charge cycle, the iron electrode was immersed in de-ionized water and then ultra-sonicated to separate the iron/copper nanoparticles from the nickel foam. The nanoparticles were then washed by de-ionized water three times and then by acetone another three times. For further analysis, the iron/copper nanoparticles were stored in acetone to prevent oxidation. The samples were identified by X-ray diffraction (XRD; Rigaku, Japan), and the morphology was observed by scanning electron microscopy (SEM; S-4700, Hitachi, Japan). Cyclic-voltammetry studies were conducted with a three-electrode cell assembly, in which the iron electrode was used as the working electrode, nickel hydroxide as the counter electrode, and Ag/AgCl as the reference electrode. Besides, the electrolyte was an 8 M KOH plus 1 M LiOH aqueous solution. Finally, cyclic-voltammetry measurements were recorded at a sweep rate of 5 mV s^{-1} and within a range from −0.2 to −1.4 V.

3. Results and discussion

3.1. Characteristics of iron and iron/copper composite nanoparticles

Fig. 1 shows the SEM images of both the pure iron (Fig. 1(a)) and the iron/copper composite (Fig. 1(b)) nanoparticles as prepared by our chemical reduction method. The particles of the pure iron have a smooth surface and sizes of about 50–150 nm, while those of the iron/copper composite system have rough surfaces and slightly large sizes of 100–200 nm. Comparing Fig. 1(b) with Fig. 1(a), we can see that a copper layer was deposited on existing iron particles. Because a part of iron was oxide and dissolved into water when the copper sulfate solution was mixed with the pure iron nanoparticles, the coating layer contained copper and some iron.

Fig. 2 shows the XRD patterns of the reduced pure iron and the iron/copper composite nanoparticles. The XRD pattern of the pure iron reveals a weak and broad peak at Fe (1 1 0), indicating

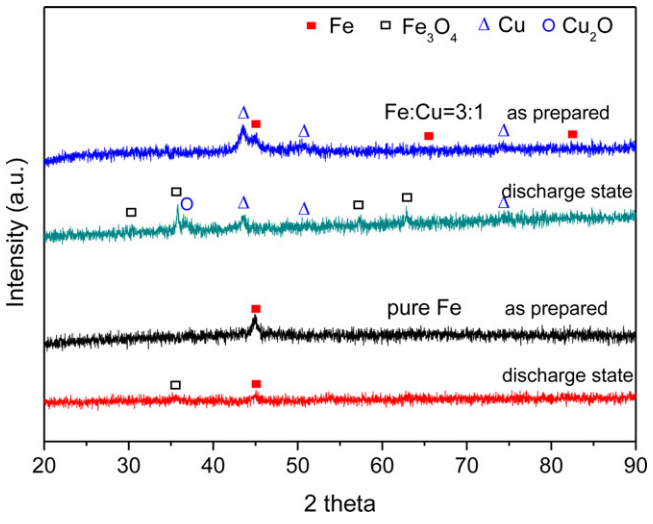

Fig. 2. The XRD patterns of the pure iron and iron/copper composite nanoparticles.

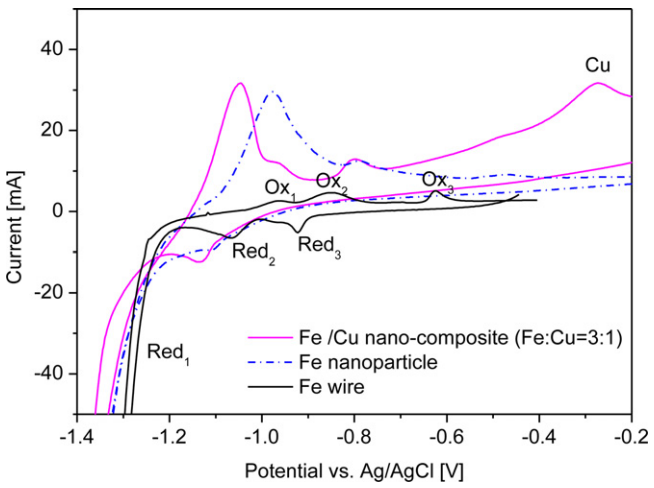

Fig. 3. Cyclic voltammetry of iron electrode materials in 8 M KOH + 1 M LiOH solution.

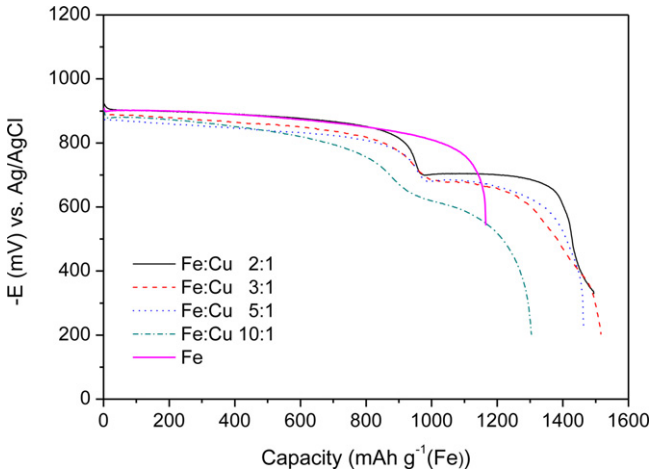

Fig. 4. Discharge curves of pure iron and various iron/copper composites. A constant current of 200 mA g^{-1} was applied at 25 °C.

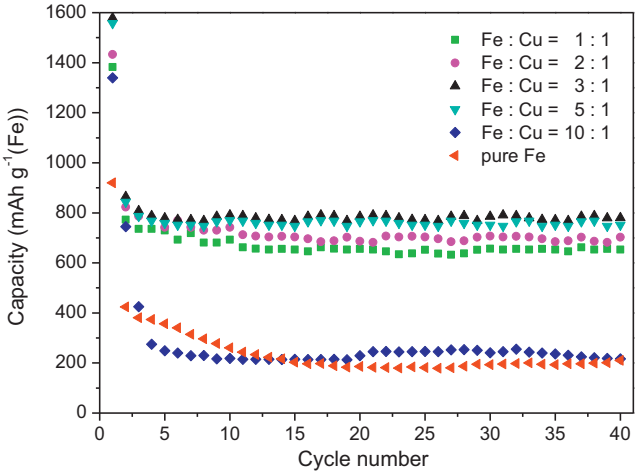

Fig. 5. Cycling stability curves of pure iron and various iron/copper composite-electrode materials at a current density 200 mA g^{-1}(Fe) between 1.65 V and 0.8 V.

a poor crystalline structure of the reduced iron nanoparticle. The iron/copper composite has weak peaks of iron and stronger peaks of copper. When both of the nanoparticles are deeply discharged, the XRD analysis of the pure iron nanoparticle shows that the peaks of iron become very weak and the peaks of Fe_3O_4 are observed, and the XRD analysis of the iron/copper composite shows that no iron remains, and the peaks of Fe_3O_4 are much stronger. Furthermore, the peak of Cu_2O was observed, indicating that some of the copper was also oxide at a deep discharge state.

Cyclic voltammograms of iron, iron/copper composite nanoparticles, as well as iron wire as the reference, are shown in Fig. 3. The curve of the iron wire involves three pairs of reduction/oxidation peaks; where the first reduction/oxidation peaks can be attributed to the reaction of Fe to $Fe(OH)_{ads}$, the second reduction/oxidation peaks are attributed to the reaction of $Fe(OH)_{ads}$ to $Fe(OH)_2$ and the third reduction/oxidation peaks are attributed to the reaction of $Fe(OH)_2$ to Fe(III) [13].

For the pure iron nanoparticle, its CV curve only shows a strong and broad oxidation peak at −0.97 V, which probably includes the reactions of Fe to $Fe(OH)_{ads}$ and $Fe(OH)_{ads}$ to $Fe(OH)_2$, but the peak corresponding to the Fe(II)/Fe(III) oxidation is not observed. The strong oxidation peak at −0.97 V implies a high reaction rate of Fe to Fe(II), and the result that very little Fe(II) would form Fe(III) is consistent with the XRD analysis.

As for the iron/copper composites, peaks at −1.03 V, −0.95 V and −0.79 V are observed in the CV curve. The first peak corresponding to the oxidation of Fe to $Fe(OH)_{ads,}$ as more negative than that of the pure iron nanoparticle (at −0.97 V) probably implies a lower over-potential. The strong oxidation peak at −0.79 V implies that the oxidation of $Fe(OH)_2$ to Fe_3O_4 is much easier. Furthermore, an oxidation peak at −0.27 V was observed, and according to the result of XRD analysis, it should correspond to the oxidation of Cu to Cu_2O.

3.2. Performance of the iron/copper composite as an electrode material

Fig. 4 displays the discharge curves of pure iron and iron/copper composite electrode materials. The first time discharge curve of pure iron had only one plateau, and suggested the conversion of Fe to $Fe(OH)_2$. The capacity was about 1100 mAh g^{-1}; greater than the theoretical value of iron of 962 mAh g^{-1}. This value probably contained contributions from other species. Because $NaBH_4$ was used as the reducing agent, the generation and incorporation of hydrogen into iron could therefore be expected [14]. During the discharge of iron ($E^0 = -0.87$ V), hydrogen could react with OH^- to produce water ($E^0 = -0.83$ V) and had made contribution to the extra electrical capacity. Since $Fe(OH)_2$ was not an electron conductor, it was unable to be further oxidized to the Fe(III) species, and hence there was only one plateau during discharge. On the other hand, the discharge curves of the iron/copper composite nanoparticles showed two plateaus. The appearance of the second plateau suggested that the presence of copper particles helped to construct the electron transfer network for the oxidation reaction of $Fe(OH)_2$ to Fe(III) species to proceed. The capacities of the iron/copper composite with the iron to copper ratios 2:1, 3:1 and 5:1 are all about 962 mAh g^{-1}(Fe) at the first plateau and 1443 mAh g^{-1}(Fe) including plateaus I and II, which are the same as the theoretical capacity of iron. The extra electrical capacity that contributed by the doped hydrogen was almost not observed, which seems to be affected by the copper depositing process. Besides, the higher amounts of copper in the composites show more flat plateaus of the discharge curve, indicating that the copper reduces the over-potential of iron electrodes.

In Fig. 5, the capacities of the electrode materials containing different amounts of copper were shown after cycles up to 40. The battery was operated between 1.65 V and 0.8 V at a current density of 200 mA g^{-1}(Fe). The capacity of the pure iron nanoparticle decreased quickly to around 200 mAh g^{-1} (Fe) at about 10 charge-discharge cycles. A corresponding increase in particle size

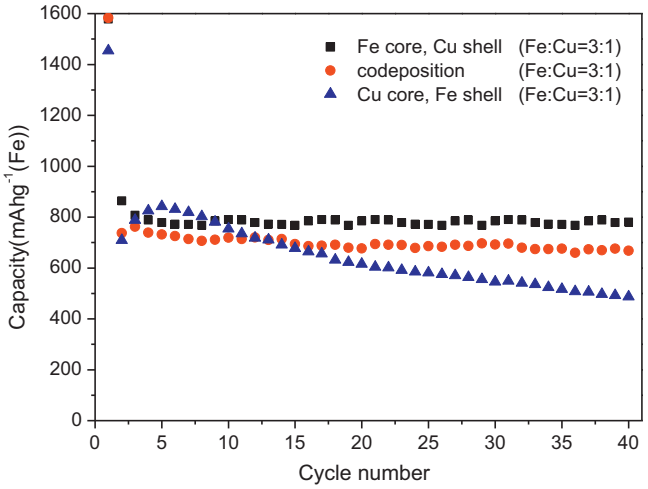

Fig. 6. Cycling performance of an iron/copper composite (Fe:Cu = 3:1) prepared by different processes at a current density of 200 mA g^{-1}(Fe) between 1.65 V and 0.8 V.

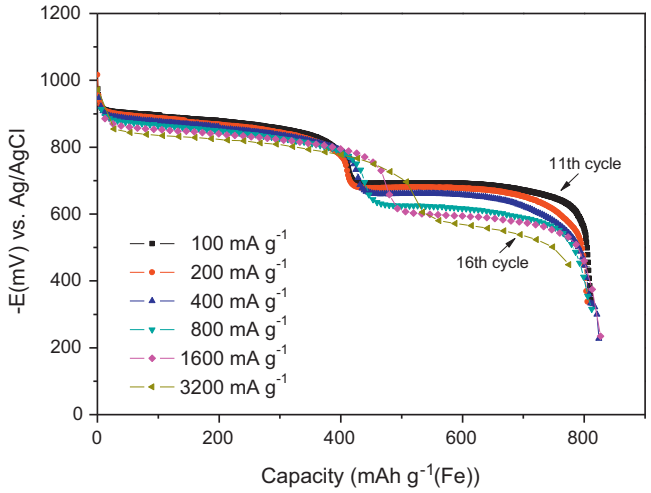

Fig. 7. Discharge curves of iron/copper composite (Fe:Cu = 2:1, in weight ratio) at various current densities.

and hence the loss of surface area was the possible reason for the decrease of electrical capacity.

The highest capacity of around 800 mAh g^{-1} was achieved when the copper addition was 1/3 (in weight) of that of iron. If the copper addition was only 1/10 of that of iron, its effect was only minimal compared with the pure iron electrode. At this stage, the copper was not enough to form an electron-conducting network to help with the oxidation/reduction electrode reactions. On the other hand, when the copper addition was over 1/3, some copper might cover the iron particle surface, and therefore the electrode exhibited a lower electrical capacity. When the addition of copper was the same as the weight of iron (i.e., 1:1), the electrical capacity was even lower at around 650 mAh g^{-1}(Fe). The value of 800 mAh g^{-1}(Fe) is a very promising number for future applications.

In this work, we prepared the iron active materials in three structures such as copper/iron core/shell, iron/copper core/shell and the coprecipitated iron and copper with the same iron to copper ratio 3:1. The cycling performances of the active materials are shown in Fig. 6. Obviously, the iron core and copper shell structure have the best performance. The coprecipitation process makes the most uniform mixing of iron and copper, but due to a poor connection of copper particles, the discharge capacity is slightly less than that of the iron core and copper shell structure. The capacity of the copper core and iron shell active material decay quickly, which is probably due to the aggregation of copper particles during its synthesizing consequently supplies fewer nuclei for the further dissolution–precipitation of iron, and also a poor connection of copper particles; therefore, the active surface area decreases gradually.

In Fig. 4, the higher amounts of copper in the composites show more flat plateaus of the discharge curve. In Fig. 5, the iron/copper composite in a weight ratio Fe:Cu = 2–5:1 discharge higher capacity. Consequently, the iron/copper composite in a weight ratio Fe:Cu = 2:1 has the best rate performance in the study, and the discharge curves at various current densities were shown in Fig. 7. It shows very few capacity lost when the discharge current density increase. Even at a very high current density of 3200 mA g^{-1}, it still discharges about 800 mAh g^{-1}.

Next, in Fig. 8, we showed the XRD patterns of pure iron and iron/copper composite at both charge and discharge state after 20 charge–discharge cycles. When the pure iron electrode discharged to 0.8 V, weak peaks of Fe and Fe_3O_4 were observed in the XRD pattern (Fig. 8(a)). In theory, the major product should be $Fe(OH)_2$ and it was not detected here, suggesting that it was amorphous. When the batteries were charged back to 1.65 V, the pure iron electrode

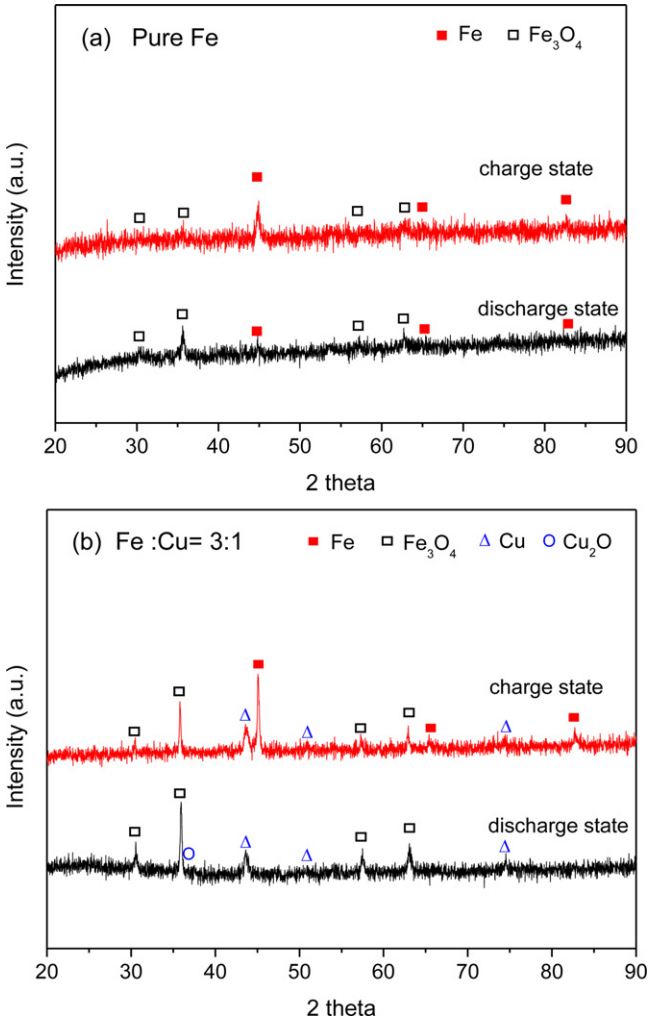

Fig. 8. The XRD patterns of the iron electrode materials at charge state and discharge state after 20 cycles: (a) pure iron; (b) iron/copper composite nanoparticles.

showed the existence of Fe and Fe_3O_4 XRD peaks. The products of $Fe(OH)_2$, FeOOH and Fe_3O_4 were poor electron conductors and were difficult to be converted back to iron, and hence the loss of capacity during the next cycle.

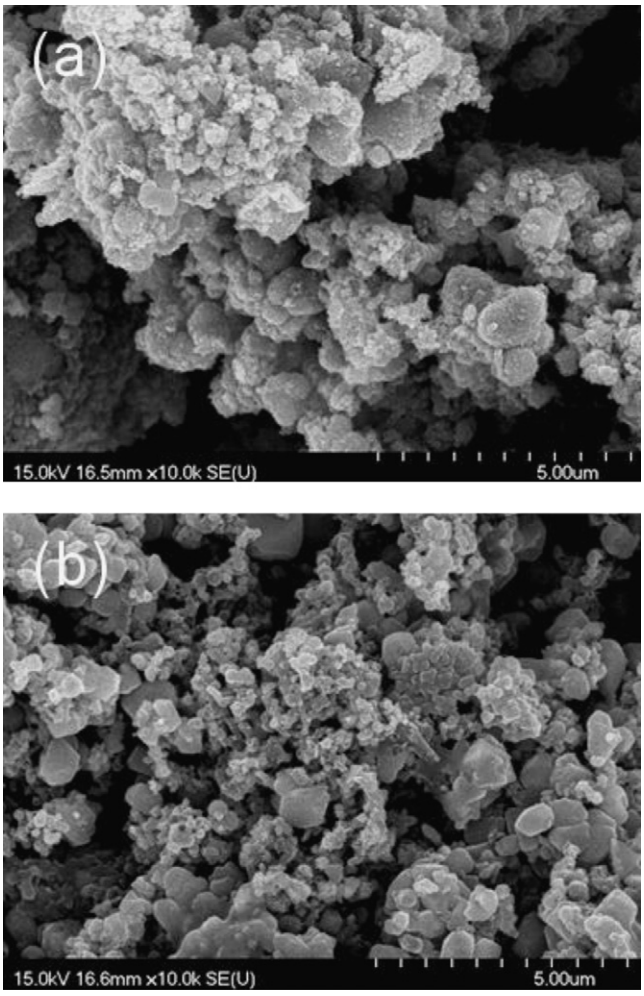

Fig. 9. SEM images of the cycled nanoparticles at charge state: (a) Pure Fe; (b) Fe:Cu = 3:1 (weight ratio).

However, when nanosized copper accompanies with the nanosized iron, only visible peaks of Fe_3O_4 and peaks of copper were detected, but not any Fe peaks at the discharge state (Fig. 8(b)). This fact seemed to suggest that the good conducting network formed by copper helped the first and second plateaus of oxidation from Fe to Fe(II) and then from Fe(II) to Fe(III). On the contrary, the electrons can also transfer to the oxidized iron species and reduce back to iron metal easily when the electrode was charged. This has helped to maintain the rough 800 mAh g^{-1}(Fe) capacity of the iron/copper electrode, while that of the pure iron electrode dropped to 200 mAh g^{-1}(Fe). However, Fe_3O_4 was still detected in the iron/copper electrode material, suggesting the inevitable loss of some iron material. Furthermore, in Fig. 7 the discharge capacity of plateau I and II are both about 400 mAh g^{-1}, which is about 42% capacity utilization rate of Fe to Fe(II) and 83% of capacity utilization rate of Fe(II) to Fe(III). Therefore, there are 41% of $Fe(OH)_2$ cannot be reduced to Fe, which can be explained by the poor charge efficiency of $Fe(OH)_2$ to Fe due to the low hydrogen over potential of nanosized iron.

Fig. 9 presents the SEM images of the pure iron nanoparticle Fig. 9(a) and the iron/copper composite nanoparticle Fig. 9(b) after 20 discharge/charge cycles. In Fig. 9(a), most particles are larger than 1 μm, and some particles aggregate as large ones. The iron/copper particles in Fig. 9(b) show a smaller particle size, and less aggregation. Besides, the surface of the particles is smoother than the particles in Fig. 9(a). When we refer to the XRD analysis in Fig. 8, we can get the result that most of the particles in Fig. 9(b) are well-crystallized iron metal, but the particles in Fig. 9(a) is of the amorphous $Fe(OH)_2$.

4. Conclusions

An anode material made up of an iron/copper composite by a chemical reduction method is successfully demonstrated to be highly reversible in this work. The copper nanoparticles in the composite construct a stable network to transfer electrons during the reduction/oxidation of the iron electrode. It therefore helps to stop the quick drop of electrical capacity due to the formation of non-conductive $Fe(OH)_2$ from iron particles. When the copper addition is higher than 1/3 (weight ratio) of that of iron, the composite electrode delivers a stable capacity of about 800 mAh g^{-1} (Fe) at a current density of 200 mA g^{-1}. The electrode material can still deliver about 800 mAh g^{-1} at a large current density of 3200 mA g^{-1}. This fact thus opens up the possibility of future applications requiring large current outputs.

Acknowledgment

The authors wish to thank National Science Council of the Republic of China, Taiwan, for financially supporting this research under Contract No. NSC 96-2628-E007-022-MY3.

References

[1] W. Feduska, R.E. Vaill, Journal of the Electrochemical Society 125 (1978) C339–C1339.
[2] D.J. Smith, W.C. Harsch, Journal of the Electrochemical Society 125 (1978) C342–C1342.
[3] E. Briner, A. Yalda, Helvetica Chimica Acta 25 (1942) 416–425.
[4] C. Chakkaravarthy, P. Periasamy, S. Jegannathan, K.I. Vasu, Journal of Power Sources 35 (1991) 21–35.
[5] A.M. Novakovs, S.A. Grushkin, R.L. Kozlova, Zhurnal Prikladnoi Khimii 46 (1973) 2183–2187.
[6] M.K. Ravikumar, T.S. Balasubramanian, A.K. Shukla, Journal of Power Sources 56 (1995) 209–212.
[7] P. Periasamy, B.R. Babu, S.V. Iyer, Journal of Power Sources 62 (1996) 9–14.
[8] K.C. Huang, S.H. Ehrman, Langmuir 23 (2007) 1419–1426.
[9] K.C. Huang, K.S. Chou, Electrochemistry Communications 9 (2007) 1907–1912.
[10] B.T. Hang, H. Hayashi, S.H. Yoon, S. Okada, J. Yamaki, Journal of Power Sources 178 (2008) 393–401.
[11] C.Y. Kao, K.S. Chou, Journal of Power Sources 195 (2010) 2399–2404.
[12] G.P. Kalaignan, V.S. Muralidharan, Bulletin of Electrochemistry 12 (1996) 213–217.
[13] J. Cerny, K. Micka, Journal of Power Sources 25 (1989) 111–122.
[14] X.F. Wang, L. Andrews, Dalton Transaction (2009) 9260–9265.